Acta Crystallographica Section B
Structural Science
ISSN 0108-7681

Crystal structures and cation ordering in $Cs_2MgSi_5O_{12}$, $Rb_2MgSi_5O_{12}$ and $Cs_2ZnSi_5O_{12}$ leucites

A. M. T. Bell[a]* and C. M. B. Henderson[a,b]

[a]Department of Photon Sciences, STFC Daresbury Laboratory, Warrington WA4 4AD, England, and [b]School of Earth, Atmospheric and Environmental Sciences, University of Manchester, Manchester M13 9PL, England

Correspondence e-mail: ynotlleb1@mac.com

Received 10 March 2009
Accepted 27 June 2009

The crystal structures of the leucite analogues $Cs_2MgSi_5O_{12}$, $Cs_2ZnSi_5O_{12}$ and $Rb_2MgSi_5O_{12}$ have been determined by synchrotron X-ray powder diffraction using Rietveld refinement in conjunction with ^{29}Si MAS NMR spectroscopy. These leucites are framework structures with distinct tetrahedral sites (*T* sites) occupied by Si and a divalent cation (either Mg or Zn in these samples); there is also a monovalent extra-framework cation (either Cs or Rb in these samples). The refined crystal structures were based on the *Pbca* leucite structure of $Cs_2CdSi_5O_{12}$, thus a framework with five ordered Si *T* sites and one ordered Cd *T* site was used as the starting model for refinement. ^{29}Si MAS NMR shows five distinct Si *T* sites for $Cs_2MgSi_5O_{12}$ and $Rb_2MgSi_5O_{12}$, but six Si *T* sites for $Cs_2ZnSi_5O_{12}$. The refined structures for $Cs_2MgSi_5O_{12}$ and $Rb_2MgSi_5O_{12}$ were determined with complete *T*-site ordering, but the refined structure for $Cs_2ZnSi_5O_{12}$ was determined with partial disorder of Mg and Si over two of the *T* sites.

1. Introduction

The crystal structure of the end-member leucite ($KAlSi_2O_6$) consists of a three-dimensional framework of silicate tetrahedra in which one third of the Si atoms are replaced by Al, with the larger (W) sites occurring in channels along [111] in this framework containing K^+ cations and the smaller (S) sites being vacant. At room temperature and pressure leucite is tetragonal and belongs to the $I4_1/a$ space group (Mazzi *et al.*, 1976). End-member pollucite ($CsAlSi_2O_6$) has K replaced by Cs giving the topologically similar $Ia\bar{3}d$ cubic structure (Beger, 1969). Analogues of these tetragonal and cubic leucite structures can also be prepared synthetically if the alkali metal cation and/or the non-silicon tetrahedral cations are replaced by other alkali metal cations and divalent or trivalent cations. This results in silicate framework structures with stoichiometries of $ACSi_2O_6$ and $A_2BSi_5O_{12}$, where *A* is an alkali metal cation (also ammonium, see Hori *et al.*, 1986), *B* is a divalent metal cation and *C* is a trivalent metal cation (Torres-Martinez & West, 1986, 1989; Bell & Henderson, 1994*a*,*b*; Bell, Henderson *et al.*, 1994; Bell, Redfern *et al.*, 1994; Palmer *et al.*, 1997). The compositional flexibility of this structure type is reviewed in Henderson *et al.* (1998).

All of these stoichiometries form phases with disordered framework cations on the tetrahedrally coordinated sites (*T* sites). However, a synchrotron X-ray powder diffraction, electron diffraction and ^{29}Si MAS NMR study of a leucite analogue with the stoichiometry $K_2MgSi_5O_{12}$ (Bell, Henderson *et al.*, 1994) showed that a dry synthesized sample had the $Ia\bar{3}d$ pollucite structure (with disordered *T* cations), but that a hydrothermally synthesized sample had a previously unknown $P2_1/c$ monoclinic leucite structure. ^{29}Si MAS NMR

and diffraction techniques on the hydrothermally synthesized sample showed that a unit cell with 24 O atoms had 12 separate T sites consisting of ten distinct Si sites [two surrounded by four SiO_4 tetrahedra, Q^4(4Si) sites, and eight surrounded by three SiO_4 tetrahedra and one MgO_4 tetrahedron, Q^4(3Si,1Mg tetrahedra) plus two MgO_4 tetrahedra, surrounded by four SiO_4 tetrahedra]. Thus, Si and Mg were ordered onto different T sites in this monoclinic structure with Mg^{2+} ions separated from each other by two silicons. Four distinct K^+ cation sites occur within this structure.

A similar synchrotron X-ray powder diffraction and ^{29}Si MAS NMR study of the leucite analogue $Cs_2CdSi_5O_{12}$ (Bell, Redfern *et al.*, 1994) established the existence of another previously unknown leucite structure which belongs to the orthorhombic *Pbca* space group based on a unit cell with 12 O atoms. ^{29}Si MAS NMR showed five distinct Si structural environments and this was used to determine that five Si and one Cd were ordered onto different T sites in this orthorhombic structure with cadmiums separated by two silicons. Two separate Cs sites occur in this structure. Rietveld refinement (Bell & Henderson, 1996) showed that other leucite analogues with stoichiometries $Rb_2CdSi_5O_{12}$, $Cs_2MnSi_5O_{12}$, $Cs_2CoSi_5O_{12}$ and $Cs_2NiSi_5O_{12}$ also had this ordered *Pbca* structure. A high-temperature X-ray powder diffraction study (Redfern & Henderson, 1996) showed that the crystal structure of hydrothermally synthesized $K_2MgSi_5O_{12}$ transformed from monoclinic $P2_1/c$ to orthorhombic *Pbca* at 622 K by a non-quenchable ferroelastic phase transition. $P2_1/c$ is a maximal subgroup of *Pbca* and it is clear that the 12 T sites in the former (in effect five pairs of silicons and one pair of tetrahedral divalent cations) are related to six T sites (five Si and one divalent cation) in the latter. *Pbca* also has half the number of Q^4(4Si) (one) and half the number of extra-framework alkali cation sites (two) compared with those in $P2_1/c$.

The space groups and tetrahedral ordering arrangements described above are completely different to those reported by Heinrich & Baerlocher (1991) for hydrothermally synthesized $Cs_2CuSi_5O_{12}$ and this phase was assigned to the tetragonal $P4_12_12$ space group with 12 O atoms, a seven T-site ordering arrangement of six Si sites [three Q^4(4Si), two half-occupied] and one Cu site, with Cu sites separated by only one Si. This structure also has three Cs sites, two half-occupied. Bell *et al.* (1993) tentatively refined $Cs_2MgSi_5O_{12}$, $Cs_2ZnSi_5O_{12}$ and $Rb_2MgSi_5O_{12}$ leucites in this tetragonal space group, but the recent acquisition of higher-resolution X-ray data, combined with existing NMR data (Kohn *et al.*, 1994), allows the re-interpretation of the structures of these phases, which is the subject of this paper.

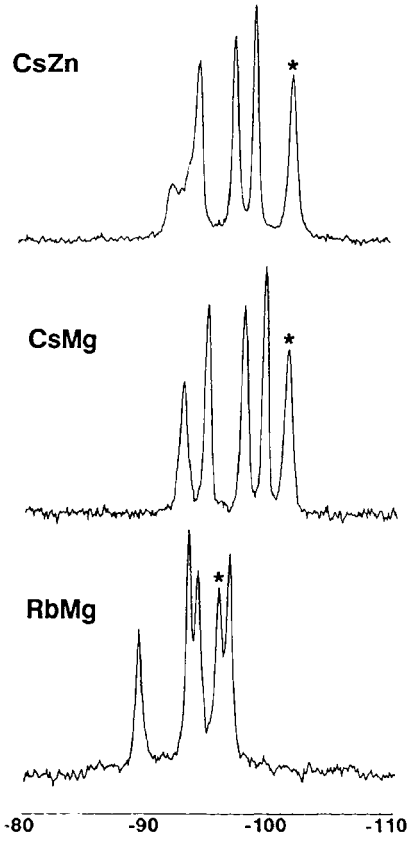

Figure 1
^{29}Si MAS NMR spectra for *Pbca* leucites; $Cs_2ZnSi_5O_{12}$ spectrum marked by CsZn; $Cs_2MgSi_5O_{12}$ spectrum marked by CsMg; $Rb_2MgSi_5O_{12}$ spectrum marked by RbMg. The asterisks mark the Q^4 (4Si) peaks (after Kohn *et al.*, 1994).

2. Experimental

2.1. Sample preparation and NMR spectroscopy

Samples of $Cs_2MgSi_5O_{12}$, $Rb_2MgSi_5O_{12}$ and $Cs_2ZnSi_5O_{12}$ were prepared from stoichiometric mixtures of Cs_2CO_3, MgO, SiO_2, Rb_2CO_3 and ZnO. These mixtures were first heated in Pt crucibles at 873 K to decompose carbonates and then melted at 1773 K ($Cs_2MgSi_5O_{12}$), 1673 K ($Rb_2MgSi_5O_{12}$) and 1683 K ($Cs_2ZnSi_5O_{12}$). The molten samples were quenched to form glasses by rapid cooling by dipping the bottom of the crucible in water; electron microprobe analysis of the glasses showed that they had the correct stoichiometries. The $Cs_2MgSi_5O_{12}$ glass was then heated in a hydrothermal cold seal bomb at 50 MPa and 1023 K for 4 d. The $Rb_2MgSi_5O_{12}$ glass was similarly heated in a hydrothermal cold-seal bomb at 50 MPa and 873 K for 28 d. The $Cs_2ZnSi_5O_{12}$ glass was crystallized at ambient pressure and 1373 K (dry synthesized) for 4.5 d. For full details of synthesis and electron-microprobe analyses for the glass starting materials see Kohn *et al.* (1994).

^{29}Si MAS NMR spectra (Kohn *et al.*, 1994) were collected on all three samples at room temperature and pressure (Fig. 1). $Cs_2MgSi_5O_{12}$ and $Rb_2MgSi_5O_{12}$ show five distinct peaks of approximately equal areas pointing to the existence of five distinct Si sites. However, $Cs_2ZnSi_5O_{12}$ shows three strong single peaks, one weaker peak and another strong peak that appears to be partially overlapped by another weaker peak. This is a more complicated Si site distribution; this has been assigned as four strong and two weak peaks, a '4 + 2' distribution.

Table 1
Experimental details.

	(1)	(2)	(3)
Crystal data			
Chemical formula	$Cs_2MgO_{12}Si_5$	$MgO_{12}Rb_2Si_5$	$Cs_2O_{12}Si_5Zn$
M_r	622.54	527.66	663.64
Crystal system, space group	Orthorhombic, *Pbca*	Orthorhombic, *Pbca*	Orthorhombic, *Pbca*
Temperature (K)	298	298	298
a, b, c (Å)	13.6371 (5), 13.6689 (5), 13.7280 (5)	13.422 (1), 13.406 (1), 13.730 (1)	13.6415 (9), 13.6233 (8), 13.6653 (9)
V (Å^3)	2559.0 (2)	2470.6 (4)	2539.6 (3)
Z	8	8	8
Radiation type	Synchrotron	Synchrotron	Synchrotron
Wavelength of incident radiation (Å)	0.993773	1.50510	0.993773
μ (mm^{-1})	18.84 (1)	–	24.21 (1)
Specimen shape, size (mm)	Cylinder, 40 × 0.7 × 0.7	Flat sheet, 30 × 1	Cylinder, 40 × 0.7 × 0.7
Specimen preparation cooling rate (K min^{-1})	700	700	700
Specimen preparation pressure (kPa)	50 000	50 000	100
Specimen preparation temperature (K)	1773	1673	1683
Data collection			
Diffractometer	In-house design	In-house design	In-house design
Specimen mounting	Capillary	Flat plate	Capillary
Scan method	Step	Step	Step
Data-collection mode	Transmission	Reflection	Transmission
2θ values (°)	$2\theta_{min}$ = 6, $2\theta_{max}$ = 75, $2\theta_{step}$ = 0.01	$2\theta_{min}$ = 10, $2\theta_{max}$ = 80, $2\theta_{step}$ = 0.01	$2\theta_{min}$ = 6, $2\theta_{max}$ = 65, $2\theta_{step}$ = 0.01
Refinement			
R_p, R_{wp}, R_{exp}, χ^2	0.114, 0.147, 0.053, 7.78	0.080, 0.101, 0.047, 4.62	0.081, 0.104, 0.062, 2.82
Excluded region(s)	2–6, 75–100° 2θ	5–10, 80–116.95° 2θ	2–6 and 65–80° 2θ
No. of data points	9801	11 196	7801
No. of parameters	67	68	69
No. of restraints	0	0	0
$(\Delta/\sigma)_{max}$	0.001	0.001	0.001

Computer programs used: local software, *CELREF* (Laugier & Bochu, 2003), *TOPAS* (Coelho, 2000), *Balls and Sticks* (Ozawa & Kang, 2004), *enCIFer* (Allen *et al.*, 2004).

2.2. Synchrotron X-ray powder diffraction

High-resolution synchrotron X-ray powder diffraction data were recently collected on $Cs_2MgSi_5O_{12}$ and $Cs_2ZnSi_5O_{12}$ samples in capillary mode at 293 K on station 9.1 of the Daresbury Synchrotron Radiation Source (SRS) with an X-ray wavelength of 0.993773 Å. Lower-resolution data on the $Rb_2MgSi_5O_{12}$ sample had already been obtained in flat plate mode at 293 K using SRS station 8.3 (Cernik *et al.*, 1990), with an X-ray wavelength of 1.50510 Å. Data were summed and normalized to account for the decay in intensity of the synchrotron X-ray beam with time.

Analysis of the powder diffraction data for all three samples showed that they could be indexed in *Pbca* with similar lattice parameters to those for leucites with the $Cs_2CdSi_5O_{12}$ structure. Intitial lattice parameters determined by *CELREF* (Laugier & Bochu, 2003) were: a = 13.6697, b = 13.6736, c = 13.7438 Å ($Cs_2MgSi_5O_{12}$); a = 13.427, b = 13.409, c = 13.735 Å ($Rb_2MgSi_5O_{12}$); a = 13.6474, b = 13.6872, c = 13.7195 Å ($Cs_2ZnSi_5O_{12}$). Note that the a and b cell parameters for all three samples are very similar and require high-resolution diffraction data, coupled with spectroscopic techniques, to deduce that they are orthorhombic rather than tetragonal.

2.3. Rietveld refinement

Rietveld refinement (Rietveld, 1969) was carried out using *TOPAS* (Coelho, 2000). For all three samples the *Pbca* leucite structure of $Cs_2NiSi_5O_{12}$ (Bell & Henderson, 1996) was used as the initial starting model for Rietveld refinement (see Table 1[1]).

2.3.1. $Cs_2MgSi_5O_{12}$. The ^{29}Si MAS NMR spectrum for this sample shows five distinct peaks of approximately equal intensity, suggesting that it has five different chemical environments for Si in its structure. As the Si:Mg ratio is 5:1, this would suggest that there are six *T* sites in this structure with Si and Mg completely ordered onto separate sites, consistent with the *Pbca* structure described above. In addition, Kohn *et al.* (1994) used ^{133}Cs NMR to show that two Cs sites are present; this is also consistent with a *Pbca* structure. The powder diffraction pattern was therefore indexed with Mg replacing Ni on the ordered non-Si *T* site in the *Pbca* starting model. As in the refinement of the $P2_1/c$ structure of $K_2MgSi_5O_{12}$ (Bell, Henderson *et al.*, 1994), *T*-site atom-to-oxygen distances were constrained initially to 1.61 (Si—O) and 1.90 Å (Mg—O). Magnesite ($MgCO_3$; Effenberger *et al.*, 1981) was included as a second phase in this refinement.

2.3.2. $Rb_2MgSi_5O_{12}$. As in the $Cs_2MgSi_5O_{12}$ sample, the ^{29}Si MAS NMR spectrum for this sample shows five distinct peaks which can be correlated with the presence of five distinct Si sites, while the ^{133}Cs NMR spectra show the presence of two

[1] Supplementary data for this paper are available from the IUCr electronic archives (Reference: HW5004). Services for accessing these data are described at the back of the journal.

Table 2
Extra-framework cation (*A*)—O distances (Å) for (*a*) $Cs_2MgSi_5O_{12}$ (*A* = Cs), (*b*) $Rb_2MgSi_5O_{12}$ (*A* = Rb) and (*c*) $Cs_2ZnSi_5O_{12}$ (*A* = Cs).

	(*a*)	(*b*)	(*c*)		(*a*)	(*b*)	(*c*)
*A*1—O1	3.81 (5)	4.01 (3)	3.84 (6)	*A*2—O1	3.40 (4)	3.16 (3)	2.92 (6)
*A*1—O2	3.89 (4)	4.27 (3)	3.79 (6)	*A*2—O2	3.69 (5)	3.56 (3)	3.80 (6)
*A*1—O3	3.86 (4)	3.74 (3)	3.29 (7)	*A*2—O3	3.81 (5)	3.91 (3)	3.47 (7)
*A*1—O4	3.71 (4)	3.71 (3)	3.85 (5)	*A*2—O4	3.68 (5)	3.47 (4)	2.75 (6)
*A*1—O5	3.56 (4)	3.66 (3)	3.63 (8)	*A*2—O5	3.31 (4)	3.49 (3)	3.77 (6)
*A*1—O6	3.51 (5)	3.52 (3)	3.45 (6)	*A*2—O6	3.86 (5)	3.53 (3)	3.69 (7)
*A*1—O7	3.05 (4)	3.14 (3)	3.40 (6)	*A*2—O7	3.22 (5)	3.13 (3)	3.64 (7)
*A*1—O8	3.25 (5)	2.92 (3)	3.38 (7)	*A*2—O8	3.46 (4)	3.34 (3)	3.92 (6)
*A*1—O9	3.25 (4)	3.22 (3)	3.59 (6)	*A*2—O9	3.46 (4)	3.54 (3)	3.82 (7)
*A*1—O10	3.41 (6)	3.10 (4)	3.38 (7)	*A*2—O10	3.82 (4)	3.87 (3)	3.69 (6)
*A*1—O11	3.62 (4)	3.55 (3)	3.45 (6)	*A*2—O11	3.59 (5)	3.15 (3)	3.50 (8)
*A*1—O12	3.16 (4)	2.92 (3)	3.83 (7)	*A*2—O12	3.57 (5)	3.82 (3)	3.49 (7)
Mean *A*1—O	3.51	3.48	3.57	Mean *A*2—O	3.57	3.50	3.54

Table 3
T—O bond lengths (Å) for (*a*) $Cs_2MgSi_5O_{12}$ (*T*1 = Mg, *T*2–6 = Si), (*b*) $Rb_2MgSi_5O_{12}$ (*T*1 = Mg, *T*2–6 = Si) and (*c*) $Cs_2ZnSi_5O_{12}$ (*T*1–2 = disordered Si/Zn, *T*3–6 = Si).

	(*a*)	(*b*)	(*c*)
*T*1—O7	1.81 (4)	1.87 (3)	1.6 (1)
*T*1—O9	1.87 (5)	1.90 (3)	1.63 (8)
*T*1—O4	1.88 (5)	1.93 (4)	1.72 (7)
*T*1—O11	1.90 (5)	1.89 (3)	1.8 (1)
Mean *T*1—O	1.87	1.90	1.69
*T*2—O5	1.59 (5)	1.65 (5)	1.74 (7)
*T*2—O1	1.60 (4)	1.57 (3)	1.75 (7)
*T*2—O10	1.63 (6)	1.62 (4)	1.77 (9)
*T*2—O3	1.63 (5)	1.62 (4)	1.86 (7)
Mean *T*2—O	1.61	1.62	1.78
*T*3—O1	1.55 (6)	1.59 (4)	1.59 (7)
*T*3—O2	1.56 (5)	1.62 (4)	1.60 (6)
*T*3—O6	1.57 (6)	1.63 (3)	1.62 (6)
*T*3—O11	1.62 (5)	1.61 (4)	1.62 (8)
Mean *T*3—O	1.58	1.61	1.61
*T*4—O2	1.55 (4)	1.60 (3)	1.60 (6)
*T*4—O12	1.57 (5)	1.63 (3)	1.60 (6)
*T*4—O3	1.59 (5)	1.56 (3)	1.61 (7)
*T*4—O4	1.60 (6)	1.59 (3)	1.66 (6)
Mean *T*4—O	1.58	1.60	1.62
*T*5—O8	1.61 (5)	1.62 (4)	1.60 (7)
*T*5—O12	1.64 (5)	1.65 (3)	1.61 (6)
*T*5—O7	1.71 (6)	1.71 (4)	1.61 (8)
*T*5—O5	1.74 (6)	1.68 (4)	1.64 (7)
Mean *T*5—O	1.68	1.67	1.62
*T*6—O6	1.57 (5)	1.58 (4)	1.59 (6)
*T*6—O8	1.60 (5)	1.59 (3)	1.60 (7)
*T*6—O9	1.61 (5)	1.63 (4)	1.61 (7)
*T*6—O10	1.67 (6)	1.66 (4)	1.63 (8)
Mean *T*6—O	1.61	1.62	1.61

Cs sites. In addition, a preliminary electron diffraction study (P. E. Champness, personnal communication) showed patterns consistent with orthorhombic *Pbca* (but not tetragonal $P4_12_12$). The sample was therefore refined using the *Pbca* starting model with Rb replacing Cs as the extra-framework cation and Mg replacing Ni as the non-Si ordered *T*-site cation. *T*-site atom-to-oxygen distances were again constrained to 1.61 (Si—O) and 1.90 Å (Mg—O). MgO (Sasaki *et al.*, 1979) was included as a second phase in this refinement.

2.3.3. $Cs_2ZnSi_5O_{12}$. In the starting model Zn replaced Ni on the ordered non-Si *T* site and *T*-site atom-to-oxygen distances were constrained to 1.61 (Si—O) and 1.93 Å (Zn—O). The non-Si *T*-site-to-oxygen distance was changed from 1.90 (Mg—O) to 1.93 Å (Zn—O) to reflect the larger four-coordinate ionic radius for Zn^{2+} (0.6 Å; Shannon, 1976.). This starting model gave an unrealistically large isotropic displacement factor for the Zn site and did not agree with the ^{29}Si MAS NMR spectrum, which shows four strong peaks and two weaker peaks. However, this '4 + 2' Si spectrum could be interpreted with a 6 *T*-site *Pbca* crystal structure with four completely ordered silicon *T* sites and two partially ordered *T* sites. Therefore, another *TOPAS* refinement was carried out with a '4 + 2' starting model. Initial starting model coordinates were taken from the $Ia\bar{3}d$ structure of pollucite ($CsAlSi_2O_6$; Beger, 1969) which were transferred to the *Pbca* orthorhombic cell. The *T* site corresponding to the ordered ('non-Si' site in the fully ordered *Pbca* structure) was given a 50:50 occupancy of Si and Zn. By analogy with Al avoidance in aluminosilicate frameworks (Loewenstein, 1954), the other partially ordered *T* site was assigned as that furthest from the first partially ordered *T* site. This too was given a 50:50 occupancy of Si and Zn. The occupancies of these partially ordered *T* sites were refined so that the sum of the Si occupancies and the sum of the Zn occupancies both equalled 1. *T*-site atom-to-oxygen distances were constrained to 1.61 (Si—O) and 1.80 Å (Si,Zn—O); the constraint distance of 1.80 Å was chosen as intermediate between distances expected for ordered tetrahedral Si—O and Zn—O distances.

3. Results

3.1. $Cs_2MgSi_5O_{12}$

The Rietveld refinement converged with R_{wp} = 0.147 and 0.4 (1) wt % of magnesite as the second phase.

Tables 2(*a*) and 3(*a*) show Cs—O and *T*—O interatomic distances (*T* = Si or Mg). Tables 4(*a*) and 5(*a*) show selected O—*T*—O and *T*—O—*T* bond angles. Fig. 2(*a*) shows the Rietveld difference plot and Fig. 3(*a*) shows a view of the crystal structure for $Cs_2MgSi_5O_{12}$ looking down the large channel in the structure (*i.e.* along [111]).

3.2. $Rb_2MgSi_5O_{12}$

The Rietveld refinement converged with R_{wp} = 0.101 and 0.62 (3) wt % of MgO as the second phase.

Tables 2(*b*) and 3(*b*) show Rb—O and *T*—O interatomic distances (*T* = Si or Mg). Tables 4(*b*) and 5(*b*) show selected O—*T*—O and *T*—O—*T* bond angles. Fig. 2(*b*) shows the Rietveld difference plot and Fig. 3(*b*) a view of the crystal structure.

Table 4
O—*T*—O bond angles (°) for (*a*) $Cs_2MgSi_5O_{12}$ (*T*1 = Mg, *T*2–6 = Si), (*b*) $Rb_2MgSi_5O_{12}$ (*T*1 = Mg, *T*2–6 = Si) and (*c*) $Cs_2ZnSi_5O_{12}$ (*T*1–2 = disordered Si/Zn, *T*3–6 = Si).

	(*a*)	(*b*)	(*c*)		(*a*)	(*b*)	(*c*)
O9—*T*1—O7	125 (2)	117 (1)	111 (5)	O3—*T*4—O12	127 (2)	120 (1)	99 (3)
O9—*T*1—O4	99 (2)	95.9 (9)	102 (4)	O3—*T*4—O4	92 (2)	100 (2)	124 (3)
O9—*T*1—O11	108 (2)	120 (1)	95 (4)	O3—*T*4—O2	94 (3)	100 (2)	120 (3)
O7—*T*1—O4	103 (2)	105.5 (9)	108 (5)	O12—*T*4—O4	128 (3)	129 (2)	105 (3)
O7—*T*1—O11	111 (2)	117 (1)	108 (5)	O12—*T*4—O2	121 (3)	104 (1)	77 (3)
O4—*T*1—O11	108 (2)	120 (1)	130 (2)	O4—*T*4—O2	85 (3)	99 (2)	114 (3)
O5—*T*2—O1	104 (3)	84 (2)	89 (3)	O7—*T*5—O12	92 (2)	88 (2)	114 (3)
O5—*T*2—O10	106 (3)	114 (1)	108 (3)	O7—*T*5—O5	120 (3)	105 (2)	113 (4)
O5—*T*2—O3	107 (3)	124 (1)	118 (3)	O7—*T*5—O8	112 (2)	121 (2)	112 (3)
O1—*T*2—O10	120 (2)	103 (1)	119 (3)	O12—*T*5—O5	107 (3)	107 (2)	102 (3)
O1—*T*2—O3	117 (3)	128 (1)	124 (3)	O12—*T*5—O8	118 (3)	122 (2)	104 (3)
O10—*T*2—O3	103 (3)	102 (2)	98 (3)	O5—*T*5—O8	107 (2)	110 (2)	111 (2)
O11—*T*3—O6	87 (3)	78 (2)	104 (3)	O9—*T*6—O10	102 (2)	96 (2)	104 (3)
O11—*T*3—O2	110 (3)	98 (1)	137 (4)	O9—*T*6—O6	115 (3)	117 (1)	121 (3)
O11—*T*3—O1	108 (3)	126 (2)	103 (2)	O9—*T*6–O8	110 (3)	103 (2)	118 (3)
O6—*T*3—O2	108 (3)	84 (1)	91 (3)	O10—*T*6—O6	97 (3)	102 (1)	100 (3)
O6—*T*3—O1	121 (3)	119 (2)	111 (2)	O10—*T*6—O8	119 (3)	112 (1)	88 (3)
O2—*T*3—O1	119 (3)	133 (1)	110 (2)	O6—*T*6—O8	114 (2)	124 (2)	117 (3)

Table 5
T—O—*T* bond angles (°) for (*a*) $Cs_2MgSi_5O_{12}$ (*T*1 = Mg, *T*2–6 = Si), (*b*) $Rb_2MgSi_5O_{12}$ (*T*1 = Mg, *T*2–6 = Si) and (*c*) $Cs_2ZnSi_5O_{12}$ (*T*1–2 = disordered Si/Zn, *T*3–6 = Si).

T—O—*T* angle	(*a*)	(*b*)	(*c*)	*T*—O—*T* angle	(*a*)	(*b*)	(*c*)
*T*2—O1—*T*3	143 (1)	119 (1)	142 (4)	*T*1—O11—*T*3	149 (1)	125 (2)	144 (3)
*T*3—O2—*T*5	138.0 (9)	134 (2)	140 (1)	*T*4—O12—*T*5	131.6 (9)	129 (2)	149 (1)
*T*2—O3—*T*5	164 (1)	148 (2)	136 (5)	Mean Si—O—Si	147	141	142
*T*1—O4—*T*5	156 (1)	167.9 (8)	130 (4)	Mean *T*1—O—*T*	143	144	143
*T*2—O5—*T*5	151 (1)	170 (2)	154 (5)	Mean *T*2—O—*T*	154	149	144
*T*3—O6—*T*6	137 (1)	131 (1)	141 (4)	Mean *T*3—O—*T*	142	127	142
*T*1—O7—*T*5	122 (1)	125 (2)	147 (3)	Mean *T*4—O—*T*	147	145	139
*T*5—O8—*T*6	150 (1)	136 (2)	139 (2)	Mean *T*5—O—*T*	139	140	147
*T*1—O9—*T*6	146 (1)	159 (2)	149 (3)	Mean *T*6—O—*T*	147	146	146
*T*2—O10—*T*6	156 (1)	158 (3)	154 (4)				

3.3. $Cs_2ZnSi_5O_{12}$

The Rietveld refinement with partial disorder on two of the *T* sites converged with R_{wp} = 0.104.

Tables 3(*c*) and 4(*c*) show Cs—O and *T*—O interatomic distances (*T* = Si or Zn). Tables 5(*c*) and 6(*c*) show selected O—*T*—O and *T*—O—*T* bond angles. Fig. 2(*c*) shows the Rietveld difference plot and Fig. 3(*c*) a view of the crystal structure.

4. Discussion

Fig. 2 shows the Rietveld difference plots for the three leucite samples; all plots have been given with *d*-spacing on the *x* axis so that refinements carried out with different synchrotron X-ray wavelengths can be compared.

Fig. 3 shows a view of all three crystal structures along [111] showing an extra-framework cation centred on a channel in the framework. All three structures are topologically the same, the channel in the $Rb_2MgSi_5O_{12}$ structure (Fig. 3*b*) appears to be slightly more collapsed than the other two owing to the smaller ionic radius of Rb^+ compared with Cs^+.

4.1. $Cs_2MgSi_5O_{12}$

The refined crystal structure gives a good fit in the Rietveld refinement with similar coordinates to those of other *Pbca* leucites related to $Cs_2CdSi_5O_{12}$. The isotropic displacement factors are all relatively small, which would be expected with a fully ordered structure. Some of the Si5 *T*—O bond lengths are slightly longer than would be expected for tetrahedrally coordinated Si—O (1.59–1.63 Å; *International Tables for X-ray Crystallography*, 1985, Vol. III), which might suggest some Si/Mg disorder on this *T* site. However, when the s.u.s on these interatomic distances are also considered, along with the five-peak ^{29}Si MAS NMR spectrum, it seems likely that this structure is completely ordered. The mean Mg—O distance is slightly smaller than that reported by Shannon (1976) for four-coordinated Mg—O (1.92 Å, assuming a radius for O^{2-} of 1.35 Å). Mean Cs—O bond lengths (Table 3*a*) are similar to those for other $Cs_2BSi_5O_{12}$ *Pbca* leucites. The mean Cs1—O and Cs2—O bond lengths are 3.51 and 3.57 Å; in comparison the corresponding bond lengths are 3.50 and 3.50 Å (*B* = Cd; Bell, Redfern *et al.* 1994), and 3.40 and 3.53, 3.42 and 3.49, and 3.46 and 3.54 Å (*B* = Mn, Ni and Co; Bell & Henderson, 1996). These Cs—O distances are all slightly larger than the mean Cs—O distance in $CsAlSi_2O_6$ leucite (3.35 Å; Palmer *et al.*, 1997), suggesting that because of the presence of the larger divalent cation the ordered framework shows a more restricted collapse around the cavity cation than the Al—Si framework.

4.2. $Rb_2MgSi_5O_{12}$

The refined crystal structure of $Rb_2MgSi_5O_{12}$ also gives a good fit for the Rietveld refinement with similar coordinates to those of other *Pbca* leucites related to $Cs_2CdSi_5O_{12}$. As in $Cs_2MgSi_5O_{12}$ the Si5—O bond lengths are slightly larger than for the other Si sites, but bearing in mind the s.u. values the difference is unlikely to be significant. Although the refined isotropic displacement factors for all the sites in $Rb_2MgSi_5O_{12}$ are relatively large, indicating some disorder, the ^{29}Si MAS NMR spectrum for $Rb_2MgSi_5O_{12}$ (Fig. 1) shows five equal intensity peaks and we conclude that this phase belongs to the fully ordered *Pbca* structure type. The mean Mg—O distance is within error of Shannon's value. Mean Rb1—O and Rb2—O bond lengths (Table 3*b*) are 3.48 and 3.50 Å, similar to those for $Rb_2CdSi_5O_{12}$ which are 3.41 and 3.45 Å (Bell & Henderson, 1996). These Rb—O bond lengths are significantly larger than the mean Rb—O distances in $RbAlSi_2O_6$ leucite

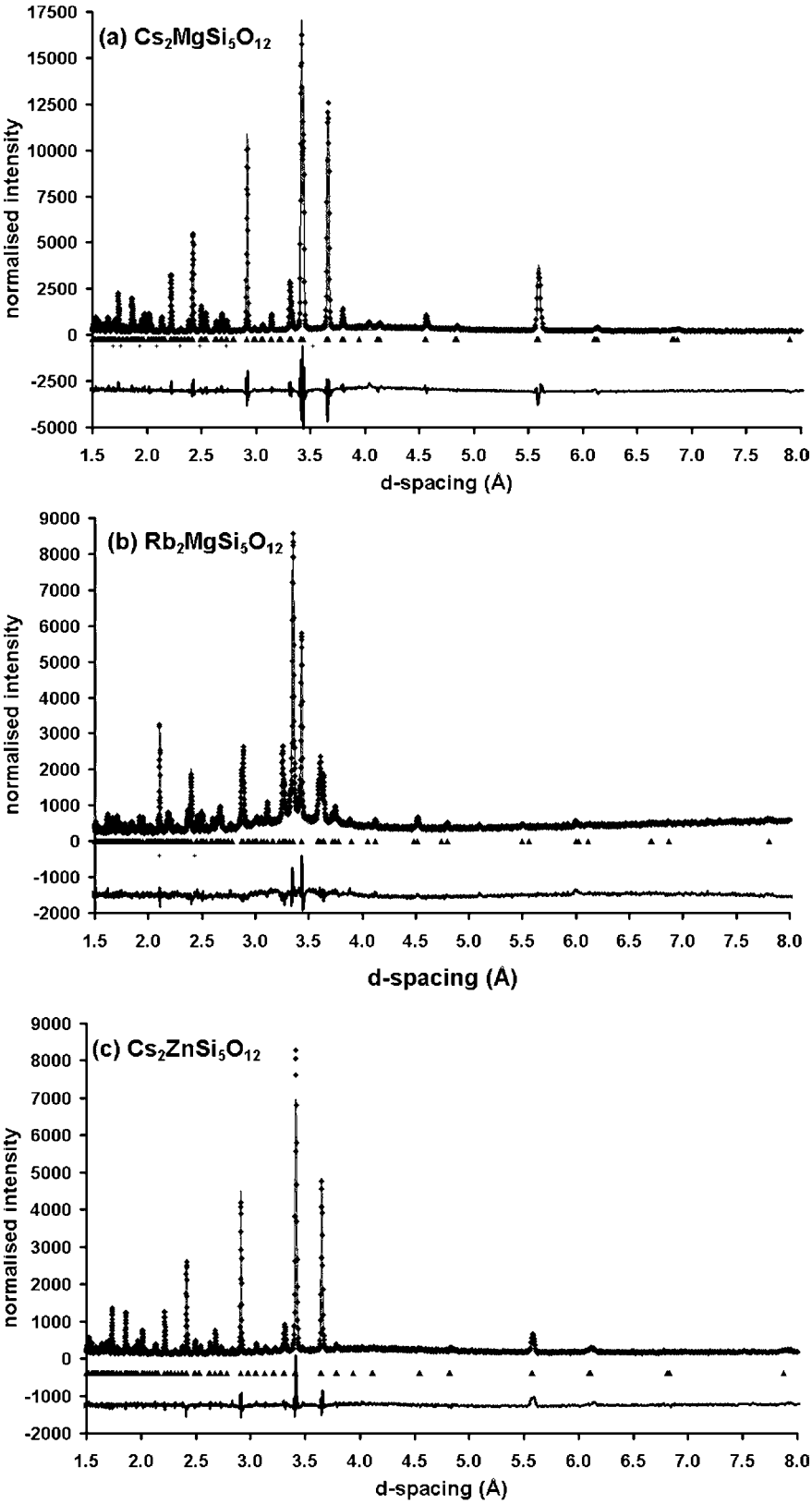

Figure 2
Rietveld difference plots for *Pbca* leucites: (*a*) $Cs_2MgSi_5O_{12}$; (*b*) $Rb_2MgSi_5O_{12}$; (*c*) $Cs_2ZnSi_5O_{12}$.

(3.14 Å; Palmer *et al.*, 1997), again reflecting the stiffer framework compared with that for Al—Si leucite.

4.3. $Cs_2ZnSi_5O_{12}$

The refined crystal structure also gives a good fit in the Rietveld refinement with similar coordinates to those of other *Pbca* leucites related to $Cs_2CdSi_5O_{12}$. Tetrahedral sites 3, 4, 5 and 6 all have mean cation–oxygen bond lengths characteristic of Si—O tetrahedra (Table 3*c*). In contrast, the *T*1—O and *T*2—O distances are intermediate to what would be expected for ordered tetrahedral Si—O and Zn—O distances. The mean *T*—O distance for the *T*1 site (1.69 Å) is closer to the ordered tetrahedral Si—O distance and the mean *T*2—O distance (1.78 Å) is closer to the ordered tetrahedral Zn—O distance. Refinement of the occupancies of the two disordered Si/Zn *T* sites gives *T*1 85 (3)% occupied by Si and *T*2 85 (3)% occupied by Zn, consistent with the mean bond lengths for these tetrahedra. Mean Cs1—O and Cs2—O bond lengths are 3.57 and 3.54 Å, similar to those for other $Cs_2BSi_5O_{12}$ *Pbca* leucites (see §4.1).

The refined isotropic displacement factors for $Cs_2ZnSi_5O_{12}$ (apart from the ordered Si *T*-site atoms) are much larger than the corresponding factors for $Cs_2MgSi_5O_{12}$ and the s.u.s on atomic coordinates and interatomic distances tend to be larger. This would be expected owing to the degree of disorder in the former phase.

Room and elevated temperature ^{29}Si MAS NMR spectra for hydrothermal $Cs_2ZnSi_5O_{12}$ led Kohn *et al.* (1994) to conclude that this sample had six Si sites at room temperature, but was close to transforming to a five Si site structure above 393 K. However, only one Q^4(4Si) peak was present while ^{133}Cs NMR spectra show the presence of two peaks (two Cs sites); such features are characteristic of the *Pbca* structure, but not a tetragonal $P4_12_12$ leucite structure which would have three Cs sites and three Q^4(4Si) sites (Heinrich & Baerlocher, 1991). The powder diffraction data show four of the *T* sites contain only Si, one (*T*1) is

Table 6
Relationship between ^{29}Si chemical shifts and mean $T-O-T$ angles for *Pbca* leucites.

Sample	NMR chemical shift	Calculated ($T-O-T$) angle S&B and Detal†	Calculated ($T-O-T$) angle (this work)‡	Measured mean ($T-O-T$) angle	T-site number
$Rb_2MgSi_5O_{12}$					
Q^4 (4Si)	−96.1	133.8	138.5	149	1
Q^4 (3Si)	−89.5	132.9	134.8	127	2
	±93.3	138.0	139.6	140	4
	−94.2	139.4	140.9	145	3
	−96.9	144.5	145.5	146	5
$Cs_2MgSi_5O_{12}$					
Q^4 (4Si)	−101.5	137.9	143.4	153	1
Q^4 (3Si)	−92.8	137.3	138.9	139	4
	−95.0	140.8	142.2	142	2
	−98.0	146.9	147.8	147	5
	−99.7	151.4	151.8	147	3
$Rb_2CdSi_5O_{12}$					
Q^4 (4Si)	−102.3	138.6	144.2	145	1
Q^4 (3Si)	±88.4	131.7	133.6	134	3
	−88.4	131.7	133.6	135	4
	−91.9	136.0	137.7	136	2
	−95.8	142.3	143.5	140	5
$Cs_2CdSi_5O_{12}$					
Q^4 (4Si)	−104.7	140.8	147.0	145	1
Q^4 (3Si)	−90.5	134.2	136.0	141	3
	−91.5	135.5	137.2	142	2
	−95.1	141.0	142.4	142	5
	−98.1	147.2	148.0	144	4
$Cs_2ZnSi_5O_{12}$					
Q^4 (4Si)	−102.3	138.6	144.2	143	1
Q^4 (3Si)	−92.4	136.7	138.4	139	4
	−93.8	138.8	140.3	142	3
	−94.6	140.1	141.6	146	6
	−97.6	146.0	146.9	147	2
	−99.2	150.0	150.5	147	5

† Q^4(4Si) $\delta = -176.7$–55.8 s (α) (Smith & Blackwell, 1983); Q^4(3Si) $\delta = -135$–31 s (α) (Dupree *et al.*, 1992) ‡ Q^4(4Si) $\delta = -176.5$–60.2 s (α); Q^4(3Si) $\delta = -140.5$–36 s (α) (this paper).

dominantly Si and the other (*T*2) contains subordinate Si. Thus, with this structure six peaks would be expected in the ^{29}Si NMR spectrum, but the relative intensities would imply five similar sized peaks and one very much smaller rather than the '4 + 2' spectrum observed (see Fig. 1). The contradictory evidence might be related to the different length-scale and time-scale characteristics of NMR and X-ray diffraction techniques and further elucidation would require further higher-resolution diffraction studies, perhaps coupled with two-dimensional ^{29}Si NMR correlation spectroscopy (COSY) experiments as carried out on $K_2MgSi_5O_{12}$ leucite (Kohn *et al.*, 1991).

In discussing the crystal chemistry of $P2_1/c$ and *Pbca* leucites, Bell, Redfern *et al.* (1994) showed how the 12 *T*-site monoclinic $P2_1/c$ structure could transform to the 6 *T*-site *Pbca* structure by combining pairs of tetrahedra. We have repeated their figure here (Fig. 4) because the earlier version had labelling errors for some of the tetrahedral species. This figure shows that the six sites in the *Pbca* structure form three pairs of *T* sites with similar connectivities and that each pair can combine to form an analogue structure with three *T* sites. It was deduced that this three-site structure would belong to the orthorhombic *Ibca* space group and that this structure must have Si and the divalent cation disordered over these three *T* sites. Note that in the structure of $Cs_2ZnSi_5O_{12}$ reported here, the *T* sites showing partial Si/Zn disorder are the Zn1 and Si2 sites and it is these sites that merge to form the T_A site in hypothetical *Ibca* leucite. It is possible that our sample is transitional in such an order/disorder transition between *Pbca* and *Ibca* structures.

5. Relationship between *T*—O—*T* angles and NMR chemical shifts in *Pbca* leucites

Various authors have addressed the empirical relationship between local crystal structure and ^{29}Si NMR chemical shifts for framework silicates (*e.g.* Smith & Blackwell, 1983; Engelhardt & Radeglia, 1984; Sherriff & Grundy, 1988; Dupree *et al.*, 1992). Smith & Blackwell (1983) used the tetrahedral framework SiO_2 polymorphs to deduce ^{29}Si chemical shift correlations with mean Si—Si bond lengths (effectively inter-tetrahedral $T-O-T$ angles) and the secant of the Si—O—Si angle and derived the relationship [$\delta = -176.7$–55.8 secant(α)], where δ is the NMR chemical shift (p.p.m.) and α is the mean Si—O—Si angle (°). The larger the $T-O-T$ angle the more negative the chemical shift.

The simplicity of any relationship will depend on the complexity of the structure (number of distinct *T* sites) and chemistry (types of different cations occupying the *T* sites) of the framework. For disordered samples very broad NMR peaks would be expected while for ordered frameworks the number of Si peaks would depend on the number of different sites. The positions of the NMR peaks depend on the local geometry of the *T* sites and the nature of the next-nearest-neighbour (NNN) tetrahedral cations. Thus, distinct peaks will occur depending on whether a particular Si is linked to four NNN tetrahedra containing Si [Q^4(4Si)], or to three, two, one or no NNN silicons [Q^4 (3Si), Q^4 (2Si), Q^4 (1Si), Q^4 (0Si)]. Clearly, different chemical shifts will occur for different *T* cations (*e.g.* Al, Mg). Dupree *et al.* (1992) derived the relationship for Q^4 (3Si,1Mg) tetrahedra in $P2_1/c$ $K_2MgSi_5O_{12}$ leucite using NMR data from Kohn *et al.* (1991) and preliminary X-ray diffraction data to be [$\delta = -135$–31 secant(α)]; note the different slope and intercept values compared with those for Q^4 (4Si) (Smith & Blackwell, 1983).

With the availability of both ^{29}Si NMR (Kohn *et al.*, 1994) and X-ray structure data (Bell, Henderson *et al.*, 1994; Bell, Redfern *et al.*, 1994; Bell & Henderson, 1996; this paper) for a range of *Pbca* and $P2_1/c$ leucite analogues it should be possible to consider the effects of different divalent tetrahedral cations (Mg, Zn and Cd) and cavity cations (K, Rb, Cs) on the relationship between chemical shift and mean $T-O-T$ angles.

However, it is not possible to carry out a rigorous analysis because we do not have detailed tetrahedral connectivity information to directly correlate a crystallographic T site with a particular NMR peak for most of the samples. We have therefore simply calculated mean $T-O-T$ angles for the Q^4 (4Si) and the four Q^4 (3Si,1B) sites in each compound and assigned the NMR peaks to these in numerical order (most negative NMR peak assigned to the largest $T-O-T$ angle). Also, the determined structures show wide ranges of individual $T-O-T$ angles for a given T site, all of which have significant errors (see Table 5). Finally, for the different *Pbca* and $P2_1/c$ leucites, there is no consistent result regarding the order of increasing mean $T-O-T$ angles for the equivalent T sites in each sample (*e.g.* see Table 6).

The equations of Smith & Blackwell (1983) and Dupree *et al.* (1992) are used to calculate mean $T-O-T$ angles from NMR chemical shifts for Q^4 (4Si) and Q^4 (3Si,1Mg), respectively, and results are summarized and compared with measured $T-O-T$ angles in Table 5 (columns 3 and 5). It is clear that there is generally very poor agreement between measured and calculated data particularly for the Q^4 (4Si) sites. We have also refitted the NMR and crystallographic data for $K_2MgSi_5O_{12}$ leucite to obtain a relationship for Q^4 (4Si) of [δ = −176.5–60.2 secant(α)]; and for Q^4 (3Si,1Mg) of δ = −140.5–36 secant(α)] (Table 6, column 4); note that the slope and intercept coefficients show some significant differences to those of Smith & Blackwell (1983) and Dupree *et al.* (1992). The calculated and measured data can be compared in Table 6 (columns 4 and 5) and show somewhat closer agreement especially for the Q^4 (4Si) sites. Any differences are presumably related to one or all of the effects of different divalent tetrahedral cations, different cavity cations, significant experimental error and perhaps incorrect assignment of NMR peaks to particular T sites. For simplicity, the experimental X-ray and NMR data are displayed in four panels in Fig. 5.

Fig. 5(*a*) shows the relationship for $K_2MgSi_5O_{12}$ and it is clear that there is no significant separation between the trends for the Q^4 (4Si) and Q^4 (3Si) trends. For each of the samples shown in Figs. 5(*b*) and (*c*), the points for the single Q^4 (4Si) tetrahedra fall close to the trends defined by the four Q^4 (3Si) species and it seems that the different NNN tetrahedral cations (Si, Mg, Cd) cause only minor perturbations to the ^{29}Si

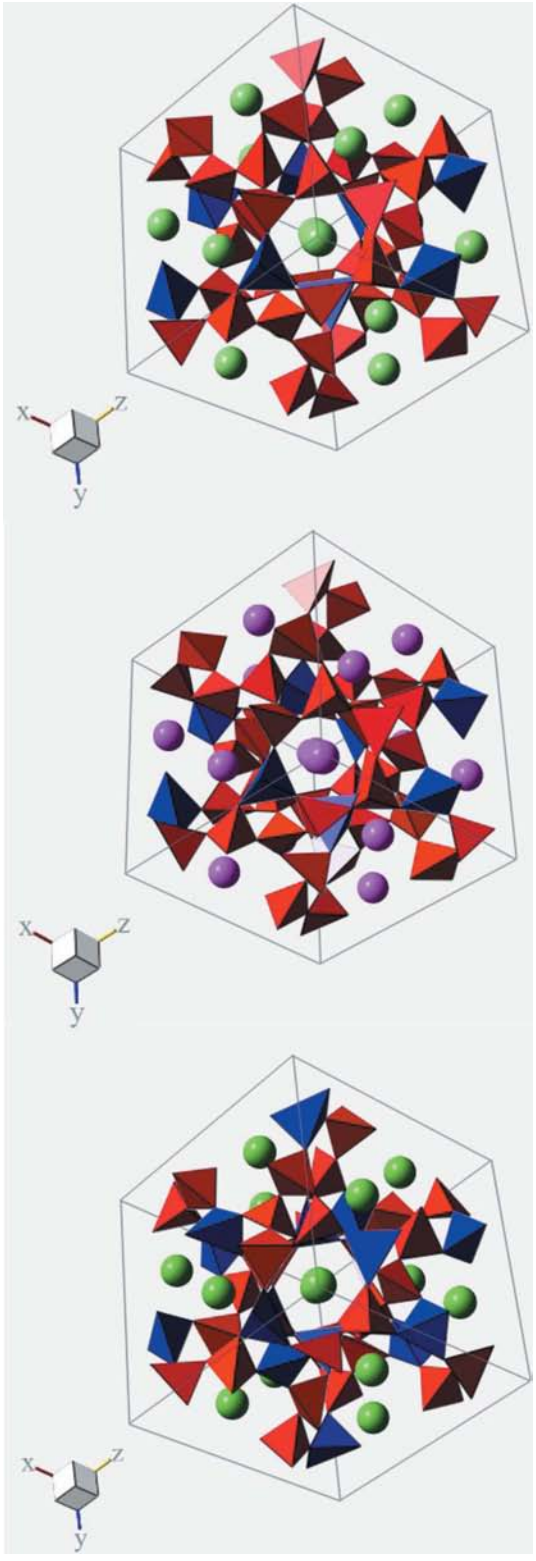

Figure 3
Crystal structures of *Pbca* leucites viewed down [111]: (*a*) $Cs_2MgSi_5O_{12}$; (*b*) $Rb_2MgSi_5O_{12}$; (*c*) $Cs_2ZnSi_5O_{12}$. Red tetrahedra are SiO_4 units and blue tetrahedra are MgO_4 units in (*a*) and (*b*), and $(Si,Zn)O_4$ units in (*c*). Plots produced using Balls and Sticks (Ozawa & Kang, 2004).

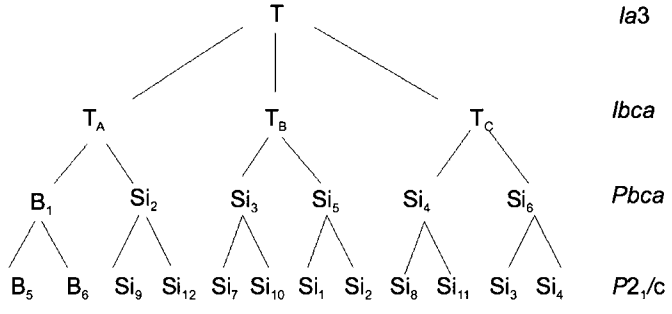

Figure 4
T-site relationships for different leucite space groups of stoichiometry $A_2BSi_5O_{12}$, where A is a univalent cavity cation and B is a divalent tetrahedral atom. The phase transitions between $P2_1/c$ and *Pbca*, and between *Ibca* and $Ia\bar{3}$ are displacive, but that between *Pbca* and *Ibca* involves tetrahedral cation order–disorder (after Bell, Redfern *et al.*, 1994).

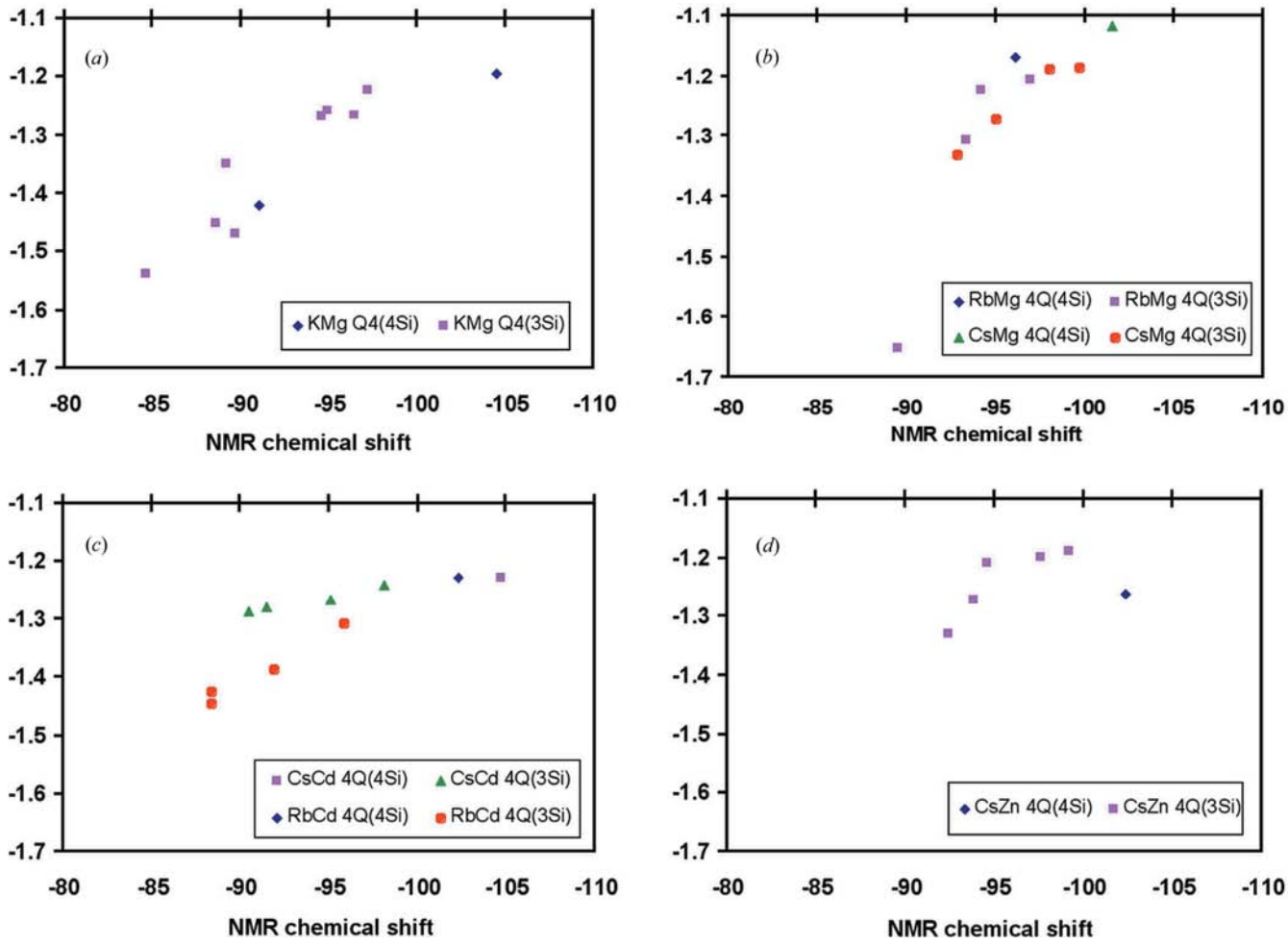

Figure 5
Plots of ^{29}Si NMR chemical shifts *versus* mean T—O—T inter-tetrahedral angles for synthetic leucites: (*a*) $P2_1/c$ $K_2MgSi_5O_{12}$ with ten Si sites [two Q^4 (4Si) and 8 Q^4 (3Si)]; (*b*) *Pbca* $Rb_2MgSi_5O_{12}$ and $Cs_2MgSi_5O_{12}$ with five Si sites [one Q^4 (4Si) and four Q^4(3Si)]; (*c*) *Pbca* $Rb_2CdSi_5O_{12}$ and $Cs_2CdSi_5O_{12}$ [one Q^4 (4Si) and four Q^4(3Si)]; (*d*) *Pbca* $Cs_2ZnSi_5O_{12}$ with four ordered Si sites and two disordered (Zn,Si) sites.

NMR chemical shifts in these samples. By contrast, and perhaps unexpectedly, it seems that the cavity cations show a bigger effect with the trends being steeper for Rb compared with those for Cs, for both Mg and Cd leucites (Figs. 5*b* and *c*, respectively). The data for $Cs_2ZnSi_5O_{12}$ are complicated by the Si–Zn disorder occurring on *T*1 and *T*2. Further work to clarify the assignment of particular NMR peaks to crystallographic *T* sites for this phase requires better structural data and a knowledge of the tetrahedral connectivities for the NMR peaks.

6. Conclusions

High-resolution synchrotron X-ray powder diffraction and ^{29}Si MAS NMR spectroscopy have been used to determine the crystal structures of leucite analogues with the stoichometries $Cs_2MgSi_5O_{12}$, $Rb_2MgSi_5O_{12}$ and $Cs_2ZnSi_5O_{12}$. The structures of $Cs_2MgSi_5O_{12}$ and $Rb_2MgSi_5O_{12}$ are similar to that for other *Pbca* leucites related to $Cs_2CdSi_5O_{12}$ and have fully ordered framework *T* sites. However, the structure of $Cs_2ZnSi_5O_{12}$ is also *Pbca*, but shows some disorder of Si and Zn on two of the 6*T* sites. The nature of the alkali cations (K, Rb, Cs) occurring in channels in the three-dimensional frameworks seems to have more effect on the inter-relationship between ^{29}Si NMR chemical shifts and mean T—O—T angles than the species of next-nearest-neighbour tetrahedral cations (Si, Mg, Cd, Zn) surrounding a central Si cation.

We wish to acknowledge the use of the Chemical Database Service at Daresbury (Fletcher *et al.*, 1996).

References

Allen, F. H., Johnson, O., Shields, G. P., Smith, B. R. & Towler, M. (2004). *J. Appl. Cryst.* **37**, 335–338.
Beger, R. M. (1969). *Z. Kristallogr.* **129**, 280–302.
Bell, A. M. T., Cernik, R. J., Champness, P. E., Fitch, A. N., Henderson, C. M. B., Kohn, S. C., Norledge, B. V. & Redfern, S. A. T. (1993). *Mater. Sci. Forum*, **133–136**, 607–702.
Bell, A. M. T. & Henderson, C. M. B. (1994*a*). *Acta Cryst.* C**50**, 984–986.
Bell, A. M. T. & Henderson, C. M. B. (1994*b*). *Acta Cryst.* C**50**, 1531–1536.

Bell, A. M. T. & Henderson, C. M. B. (1996). *Acta Cryst.* C**52**, 2132–2139.
Bell, A. M. T., Henderson, C. M. B., Redfern, S. A. T., Cernik, R. J., Champness, P. E., Fitch, A. N. & Kohn, S. C. (1994). *Acta Cryst.* B**50**, 31–41.
Bell, A. M. T., Redfern, S. A. T., Henderson, C. M. B. & Kohn, S. C. (1994). *Acta Cryst.* B**50**, 560–566.
Cernik, R. J., Murray, P. K., Pattison, P. & Fitch, A. N. (1990). *J. Appl. Cryst.* **23**, 292–296.
Coelho, A. (2000). *TOPAS*, Version 2.1, http://www.topas-academic.net/.
Dupree, R., Kohn, S. C., Henderson, C. M. B. & Bell, A. M. T. (1992). *NATO ASI*, **386**, 421–430.
Effenberger, H., Mereiter, K. & Zemann, I. (1981). *Z. Kristallogr.* **156**, 233–243.
Engelhardt, G. & Radeglia, R. (1984). *Chem. Phys. Lett.* **108**, 271–274.
Fletcher, D. A., McMeeking, R. F. & Parkin, D. J. (1996). *Chem. Inf. Comput. Sci.* **36**, 746–749.
Heinrich, A. R. & Baerlocher, Ch. (1991). *Acta Cryst.* C**47**, 237–241.
Henderson, C. M. B., Bell, A. M. T., Kohn, S. C. & Page, C. S. (1998). *Mineral. Mag.* **62**, 165–178.
Hori, H., Nagashima, K., Yamada, M., Miyawaki, R. & Marubashi, T. (1986). *Am. Mineral.* **71**, 1022–1027.
Kohn, S. C., Dupree, R., Mortuza, M. G. & Henderson, C. M. B. (1991). *Phys. Chem. Miner.* **18**, 144–152.
Kohn, S. C., Henderson, C. M. B. & Dupree, R. (1994). *Phys. Chem. Miner.* **21**, 176–190.
Laugier, J. & Bochu, B. (2003). *CELREF*, Version 3, http://www.ccp14.ac.uk/tutorial/lmgp/CELREF.htm.
Loewenstein, W. (1954). *Am. Mineral.* **39**, 92–96.
Mazzi, F., Galli, E. & Gottardi, G. (1976). *Am. Mineral.* **61**, 108–115.
Ozawa, T. C. & Kang, S. J. (2004). *J. Appl. Cryst.* **37**, 679.
Palmer, D. C., Dove, M. T., Ibberson, R. M. & Powell, B. M. (1997). *Am. Mineral.* **82**, 16–29.
Redfern, S. A. T. & Henderson, C. M. B. (1996). *Am. Mineral.* **81**, 369–374.
Rietveld, H. M. (1969). *J. Appl. Cryst.* **2**, 65–71.
Sasaki, S., Fujino, K. & Takeuchi, Y. (1979). *Proc. Jpn Acad.* **55**, 43–48.
Shannon, R. D. (1976). *Acta Cryst.* A**32**, 751–767.
Sherriff, B. L. & Grundy, D. (1988). *Nature*, **332**, 819–822.
Smith, J. V. & Blackwell, C. S. (1983). *Nature*, **303**, 223–225.
Torres-Martinez, L. M. & West, A. R. (1986). *Z. Kristallogr.* **175**, 1–7.
Torres-Martinez, L. M. & West, A. R. (1989). *Z. Anorg. Allg. Chem.* **573**, 223–230.